X-661-76-119
PREPRINT

HOT INTERSTELLAR TUNNELS: I. SIMULATION OF INTERACTING SUPERNOVA REMNANTS

BARHAM W. SMITH

MAY 1976

GSFC
GODDARD SPACE FLIGHT CENTER
GREENBELT, MARYLAND

X-661-76-110

HOT INTERSTELLAR TUNNELS:

I. SIMULATION OF INTERACTING

SUPERNOVA REMNANTS

Barham W. Smith*

Space Physics Laboratory, University of Wisconsin

and

Laboratory for High Energy Astrophysics, Goddard Space Flight Center

*NAS-NRC Resident Research Associate

Revised May 1976

GODDARD SPACE FLIGHT CENTER
Greenbelt, Maryland

ABSTRACT

Reexamining a suggestion of Cox and Smith (1974), it is found that intersecting supernova remnants can indeed generate and maintain hot interstellar regions with $n \leqslant 10^{-2}$ cm^{-3} and $T \sim 10^{6}$ K. These regions are likely to occupy at least 30% of the volume of a spiral arm near the midplane of the gaseous disk if the local supernova rate there is greater than 1.5×10^{-7} Myr^{-1} pc^{-3}. Their presence in the interstellar medium is supported by observations of the soft X-ray background.

The theory required to build a numerical simulation of interacting supernova remnants is developed. The hot cavities within a population of remnants will become connected, with varying ease and speed, for a variety of assumed conditions in the outer shells of old remnants. Rayleigh-Taylor instabilities are important in forming connections. Apparently neither radiative cooling nor thermal conduction in a large-scale galactic magnetic field can destroy hot cavity regions, if they grow, faster than they are reheated by supernova shock waves, but interstellar mass motions disrupt the contiguity of extensive cavities necessary for the dispersal of these shocks over a wide volume.

Monte Carlo simulations show that a quasi-equilibrium is reached in the test space within 10^{7} yrs of the first supernova and is characterized by an average cavity filling fraction of the interstellar volume. Aspects of this equilibrium are discussed for a range of supernova rates. Two predictions of Cox and Smith are not confirmed within this range: critical growth of hot regions to encompass the entire medium, and the efficient quenching of a remnant's expansion by interaction with other cavities.

CONTENTS

HOT INTERSTELLAR TUNNELS: I. SIMULATION OF INTERACTING SUPERNOVA REMNANTS

I. INTRODUCTION

It has been suggested by Cox and Smith (1974; hereafter CS) that intersections of supernova remnants contribute to the production of gas at about 10^6 K which is apparently observed in the interstellar medium. Evidence for this gas was first found at low galactic latitudes in soft X-ray emission exceeding the extrapolated diffuse background determined at higher energies (e.g. Bunner, et al. 1972). Kraushaar (1973) and Williamson, et al. (1974) have concluded that the soft X-ray observations require widespread thermal emission regions interwoven with cooler gas, because of the short mean free path for 250 eV photons in interstellar gas (Brown and Gould 1970) and because a broad range of other emission mechanisms can be eliminated. The analysis of ultrasoft X-ray observations by Levine, et al. (1976) is also consistent with this hypothesis. Since Vanderhill, et al. (1975) and others have set fairly stringent upper limits on the space densities of soft X-ray stars, the diffuse soft background seems to require hot interstellar gas. Contrary to early expectations (CS), ultraviolet observations of O VI interstellar absorption lines in the spectra of unreddened hot stars, e.g. Jenkins and Meloy (1974) and York (1974), give no unambiguous evidence for this gas, since the observed absorption may be associated with the stars themselves (Castor, McCray, and Weaver 1975). However, the latter

work does not weaken the X-ray evidence, since hot gas produced by these uncommonly hot stars (earlier than ~B2; Snow and Morton 1976) cannot supply the diffuse soft X-ray background (McCray 1976). Moreover, Scott (1975) has recently given substance to the suggestion in CS that very hot regions may be preferred channels for cosmic ray propagation, and he points out that fresh estimates of cosmic ray lifetimes in the Galaxy favor this idea, although he oversimplified the problem.

These considerations justify a continued exploration of the ideas of CS. The fundamental prediction of the CS model is that intersections of supernova remnants (SNRs), which involve the interaction of older low-density cavities left by SNRs with strong shock fronts of other supernovae (SNe), generate more hot gas from an initially cold interstellar medium (ISM) than in the absence of interactions. A high SN rate per unit volume or a population of very-large-diameter SNRs might generate enough hot gas to satisfy the X-ray observational demand by simple superposition, but it turns out that overlaps, interactions, and cooperative regeneration of remnants are still likely to occur. In this paper the important physical processes encountered in the model are discussed.

A fairly detailed numerical simulation of interacting SNRs has been developed, and a description of its design and results occupy the latter half of the paper. The complex geometry and competing processes which connect and rejuvenate remnants can only be treated by numerical simulation except in the most trivial cases. We have investigated the large-scale three dimensional

behavior of a test section of the gaseous galactic disk under the influence of evolving and interacting SNRs. The accuracy of the method rests on the validity of models for individual and collective SNR behavior. Ultimately the models must come from separate gas-dynamical calculations, although even when such results are available the complexity of the simulation forces simplification of the models. Thus the simulation should provide reliable global properties of the medium but not detailed information about small-scale local structure. The chief aim of the discussion here will be to show that SNR intersections can quickly generate large volumes or "tunnels" of very hot gas from a cold starting medium, under conservative and reasonable assumptions. The two most important ones, explained later, are that SNRs can be treated as spheres and that mass motions may be treated implicitly.

In the next few sections the SNR models selected as building blocks for the simulation are assembled. First, in §II models for a noninteracting, "isolated" SNR and the ambient medium are discussed. §III examines pairs of interacting remnants and the mechanism by which their central cavities can become connected, while §IV deals with the evolution of larger aggregates of remnants. After these developments, the simulation will be described in §V and its results presented and discussed in §VI. Conclusions are summarized in the final section.

II. ISOLATED SUPERNOVA REMNANTS

a) Very Late Remnant Evolution

The SNR radius of interest for the SNR connection mechanism of CS is not the shock radius R_s but the inner radius R_i which delimits the hot, low-density central cavity (see Cox 1972 for an overview of SNR evolution). In old remnants R_i is the inner radius of the dense shell which forms around the cavity. The cavity must be reached by another SNR shock before a connection can proceed. There are many uncertainties in the later evolution of R_i, but the particular evolution chosen here is sufficient to portray the general behavior of all solutions with respect to connections.

Spherically symmetric models such as Model A of Chevalier (1974) can be extrapolated in time with some confidence to the point where the interior pressure P_i (which is well defined because of the high sound speed in the cavity) equals the ambient pressure P_{ISM}, under the assumption that the dense shell remains hydrodynamically stable. This point is normally reached by an age of 10^6 yrs, when the final radius R_{if} is in the range 35 - 70 pc, depending weakly on the initial blast energy E_0 ($\lesssim 10^{51}$ ergs) and the ambient density n_0 ($\gtrsim 0.1$ cm^{-3}). Due to the residual momentum of the dense shell, the cavity may actually expand beyond the pressure equilibrium point. Then P_i would drop below P_{ISM}, since the rate at which edge material can be accelerated inward by external (interstellar) pressure is inadequate to enforce pressure equilibrium. In the present work isolated remnant sizes will be restricted to the smaller and simpler regime.

The representative SNR evolution which will be used exclusively for the remainder of this paper is given in Table 1. It is Chevalier's (1974) Model A scaled up to $E_0 = 6\times10^{50}$ ergs and $n_0 = 0.7$ cm^{-3} by the method described in his paper. For each value of the remnant age $t_5 \equiv t/10^5$ yrs, the shock radius and speed and the fraction of E_0 remaining as thermal energy in the hot cavity, E_i/E_0, are given in columns 2 through 4. These quantities were taken from Chevalier's Figure 1 as far as possible and then extrapolated using his power law fits and assuming the later expansion of the cavity to be adiabatic. Assuming only that the mean pressure in the dense shell (which forms just before $t_5 = 1.0$) is proportional to the ram pressure of material entering the shock, one can calculate the mean density compression factor in the shell $\langle x \rangle = \langle n_{shell} \rangle / n_0$, column 5. Since essentially all the SNR mass then resides in the shell, mass conservation gives the shell thickness ΔR and implies an inner radius $R_i = R_s - \Delta R$. Finally the cavity pressure is $P_i = E_i / 2\pi R_i^3$.

Taking account of the continued accretion of cavity gas onto the inside of the dense shell (which does not cause significant departures from the adiabatic drop of E_i), one finds a cavity density $n_i \lesssim 10^{-2} n_0$ at R_{if}. With this density at P_{ISM}, the isobaric cooling time is quite long. It turns out that a faster "destruction" of the contiguous, low-density region within a SNR may occur when it is pinched off or bridged and becomes disconnected into separate volumes by motions of cooler gas. Therefore a cavity may "die" for purposes of the CS model after a time of roughly

$$\tau_{SNR} \sim 4 \left(\frac{R_{if}}{40 \text{ pc}} \right) \left(\frac{10 \text{ km s}^{-1}}{v_{gas}} \right) \text{ Myr.} \qquad (1)$$

To simplify interpretation of the simulation results, $\tau_{SNR} = 4$ Myr has always been used. But if SNR connections become frequent, some cavities are never destroyed, in the sense that the low-density regions never completely disappear.

b) Cloud Structure

Realistic models of the ISM should take its density inhomogeneities into consideration in a self-consistent way. For example, the evolution of SNRs depends qualitatively on the cloud structure of the ambient medium. Clouds which are small in the dimension parallel to a shock velocity, as well as all sufficiently low-mass clouds, are accelerated by the SNR shock passage and the postshock flow, becoming part of the kinetic energy field of the remnant and eventually joining the dense shell. In contrast, massive or monolithic clouds left behind the shock do not seriously affect its dynamics (McKee and Cowie 1975, Sgro 1975). Thin filamentary or lamellate clouds are probably responsible for some of the 21-cm emission and absorption (Heiles 1973, Verschuur 1974; cf. Greisen 1976, Spitzer and Jenkins 1976). In a study of conditions in hot regions Shapiro and Field (1976) derive a high pressure which implies that some H I clouds used to obtain P_{ISM} could be lamellate rather than spheroidal. In fact, thin cloudlets arise inevitably from abundant interstellar shocks due to SNe themselves, as well as stellar winds, nova outbursts, etc. Elmergreen

(1975, 1976) argues that the ionized intercloud density is of order 1 cm^{-3} . A consistent picture of the cycle of gas, "evaporated" from clouds by stellar ultraviolet to form (clumpy) intercloud material and then swept up by shocks into new clouds, would include thin clouds as a prominent stage because of thermal instabilities behind shocks (Chevalier and Theys 1975; McCray, Stein, and Kafatos 1975). Therefore if one is practically constrained to uniform-density SNR models (such as Chevalier 1974), one should use a value of n somewhere between the average and intercloud densities, as we have here.

Note that McKee and Cowie claim that only the filling fraction of clouds is important for evaluating their dynamical effect on SNRs: We contend that the density which can be quickly accelerated by the shock is the significant quantity, and that it depends on cloud morphology.

A significant consequence of the flattening of clouds swept up by shock fronts is that the embedded magnetic fields tend to be compressed and aligned chiefly parallel to the filaments and sheets. Heiles (1973) has discussed observations which support this expectation. This alignment affects transport properties between clouds and hot regions, and it may also mean that a magnetic field contrast can be maintained.

c) Thermal Conduction

The conduction of heat from hot, low-density regions to surrounding or included cooler regions probably does not critically affect the survival of the hot regions. Let us consider two possible effects in turn.

Does a hot, old SNR cavity cool by losing heat to its dense shell? The thermal conductivity in the absence of a magnetic field for $T \sim 10^6$ K is (Spitzer 1962)

$$\kappa_0 \sim 6 \times 10^{-7} T^{5/2} \text{ erg s}^{-1} \text{ cm}^{-1} \text{ K}^{-1} . \quad (2)$$

The conductivity perpendicular to a magnetic field is decreased by

$$\frac{\kappa_\perp}{\kappa_0} \sim 3 \sim 10^{-11} \left(\frac{n_p}{B}\right)^2 T^{-3} , \quad (3)$$

where n_p is the proton density and B is in μG. If the dense shell of an old remnant has expanded in the presence of a large-scale field component B_0 which is uniform over scales larger than a remnant, then the shell will have a parallel field component everywhere except at two small "caps." When conduction to the shell is predominantly perpendicular to the shell field, solution of the heat flow equation (e.g. Spitzer 1956) with $\kappa_\perp$ shows that heat transport in this situation is utterly negligible. The unit area of the shell where frozen-in field lines might directly connect the hot interior and the cold shell gas can be estimated from flux-freezing:

$$\frac{A_{cap}}{\pi R_i^2} \sim \frac{B_i}{B_0} \sim \left(\frac{n_i}{n_0}\right)^{2/3} \lesssim 10^{-4/3} . \quad (4)$$

Over these small areas, heat flow is one dimensional and along the field, so the heat flow equation can be solved for the energy flux, using Spitzer's (1956) method. Mass flow is neglected, pressure equilibrium at 10^{-12} dyn cm^{-2} is assumed, and a recent radiative cooling coefficient* is used. For a typical cavity temperature of 10^6 K the quasi-steady conduction region is ~ 11 pc thick and the conduction cooling time is

$$t_{cond} \sim \frac{19}{N} \left(\frac{E_i}{2 \times 10^{49}}\right) \left(\frac{300}{A_{cap}}\right) \text{Myr} , \qquad (5)$$

where E_i is in ergs and A_{cap} in pc^2 . N is the number of unit exchange areas over which field-free conduction is established; N = 2 for a spherical SNR with "caps" but no included clouds threaded on the cavity field.

Does "evaporation" of clouds destroy cavities? Chevalier (1975) claims that evaporation of "standard" clouds will cool a cavity in the total absence of magnetic fields in $< 10^6$ yrs. Since fields are probably present, (4) estimates the upper limit to a unit field-free exchange area for a standard cloud, unless better estimates become available from detailed studies of the heat flow problem such as Cowie and McKee (1976). These authors have reached conclusions different from Chevalier's, finding that saturation of conductivity and the sensi-

*$L(T) \sim 1.2 \times 10^{-19} T^{-1/2}$ erg cm^3 s^{-1} is an excellent approximation for $3 \times 10^5 < T < 5 \times 10^7$K to the total cooling curve of Raymond, Cox, and Smith (1976) and recovers the same temperature dependence as that deduced by Spitzer (1956).

tivity of cloud evaporation rates to the hot gas temperature prevent even embedded "standard" clouds unshielded by magnetic fields from cooling a hot region much below 10^6 K. Moreover, thin clouds may be much less affected by conduction. In view of this controversy, we may appeal to soft X-ray observations as suggested by Chevalier (1975) to reassure us that considerable gas at $\sim 10^6$ K does survive conduction cooling. However, note also that the arguments of McKee and Ostriker (1975) suggest that only by admitting some cloud evaporation can one keep interacting SNR cavities from thermal runaway toward higher temperatures; new SNRs occurring in low-density regions have higher cavity temperatures than the first SNRs in a cold medium.

III. CONNECTIONS BETWEEN CAVITIES

The probability P_{in} that a new SN occurring at random will be inside an old remnant cavity is equal to the fraction f of the volume occupied by cavities at that time. If SNRs do not intersect, f is equal to $1 - e^{-q}$, where q is the dimensionless porosity defined in CS:

$$q \equiv r \tau_{SNR} V_{SNR} , \qquad (6)$$

where r is the SN rate per unit volume and $V_{SNR} = 4 \pi R_{if}^3/3$. For large q, intersections are inevitable, and $f \neq 1 - e^{-q}$. Porosity has a simple meaning for $q << 1$, so that intersections are rare, namely $f = p_{in} \approx q$. Those SNe which do not occur inside cavities may yet occur near enough to a cavity to

burst into it. Let us consider how cavities are rejuvenated and/or connected for these two types of interactions, i.e. for SNe inside and outside cavities.

The outcome of a SN event inside a remnant cavity is a shock expanding rapidly through low-density gas out to the edge; cf. Chevalier's (1974) model with $n_0 = 10^{-2}$ cm^{-3} or Cowie (1976). The old cavity will be strongly reheated, and the resulting general repressurization would give a renewed impetus to an enclosing dense shell. If cold inclusions are present in the cavity, the strong shock will go around them to reach all the low-density volume, and it will drive into them as into the dense rim of the cavity. The rejuvenation of the cavity is due to reheating of cavity gas and to compression of dense inclusions. Clouds struck by shocks have been considered by McKee and Cowie (1975) and Sgro (1975). McKee and Cowie concentrate on the "main" cloud shock structure. Sgro's numerical results show that the shock enters a dense cloud from all sides, and tends to keep it compressed if the postshock cloud gas radiatively cools before the cloud is completely shocked. Less dense clouds reexpand sooner. The critical cloud density is given, using Sgro's notation but the more recent L(T) given in §II, by $n_c'/n \sim 10^{-3}\ (nd)^{-1/3}\ \beta^{2/3}\ v_s^{4/3}$, where n is the low cavity density and n_c' is the corresponding critical value of the cloud density. The size of the cloud is d pc, v_s is in km s^{-1}, and $\beta \geq 1$ is the ratio of postshock pressures inside and outside the cloud, discussed both by Sgro and by McKee and Cowie. For $n \sim 10^{-2}$, $d = 5$, and $v_s = 1000$, inclusions with $n_c \gtrsim 1$ cm^{-3} should remain relatively compressed after the shock passes.

With respect to the cavity demise represented by equation (1), shocks forestall the filling, bridging, and pinching off of cavities by clouds; since the actual lifetime thereby added to a cavity is difficult to pin down quantitively, a range of rejuvenation hypotheses should be studied.

If a SN occurs outside a cavity but nearby, and if the strong shock front of the young SNR considerably overlaps the cavity, at least one low-density channel may be opened between the two cavities. Such channels, forming a "connection," ensure that a later shock propagating through one cavity will propagate through the connection into the other, providing a rejuvenating effect similar to that outlined above. The establishment of the connection takes some time, during which the newer SNR expands normally, but if its interior pressure is diverted through a channel before its shell forms, this remnant may not reach its full normal size.

How do these channels come about? Dense gas in an old SNR shell which is struck from the outside by a shock is first accelerated suddenly as the front passes, and then further accelerated and decelerated in a complex way which depends on the density structure through the shell. When the shock speeds up into lower density on the far side of the shell, a rarefaction wave propagates back through the shell. With pressure differences across the shell of more than factors of 10^2 on top of the various accelerations, it is plausible that the shell is subject to Rayleigh-Taylor instabilities. Full calculations, which take into account the effect of compressibility emphasized by Chevalier and Theys

(1975), are quite difficult to perform for these instabilities, but we can estimate the magnitude of the connection time delay using the approximate treatment of Frieman (1954). This assumes a static, incompressible, nonviscous fluid subject to an acceleration. Idealize the situation as follows: When the new shock hits the old shell, the shock speed drops suddenly and a reflected shock forms, increasing the thermal pressure between the shocks. If the average shock speed in the shell is v_s, then the transmitted shock takes a time $t_{cross} \sim \Delta R/v_s$ to cross the shell. For the important case in which the younger active SNR can still be described by a Sedov adiabatic blast wave and has no shell, Table 1 gives $t_{cross} \lesssim 10^5$ yrs. The thermal pressure difference ΔP across the shell is sufficient to cause an instability after t_{cross} has elapsed and P_i of the new remnant has meanwhile dropped from overall expansion. This ΔP implies an effective gravity $g \sim \Delta P/\rho_s \Delta R$, where ρ_s is the average shell density and $\rho_s \Delta R$ is constant during the compression of the shell by the crossing shock. A rough lower bound for g under conditions favorable to connection is 4 km s^{-1} $(10^5$ yr$)^{-1}$. The dispersion relation for the instability can be written (Frieman 1954) $\lambda \sim 2\pi g t_{R-T}^2$, where t_{R-T} is the growth time in the linear regime and λ is the scale (both parallel and perpendicular to the shell) over which the instability has grown after an elapsed time t_{R-T}. As an indication that the shell ruptures we require $\lambda \sim \Delta R$, calculating a growth time $t_{R-T} \sim 10^5$ yrs. Comparing $t_{cross} + t_{R-T}$ to time scales for SNR evolution, and recognizing that

the two delays overlap somewhat if the instability sets in during t_{cross}, one can conservatively conclude that some SNR intersections result in connections.

However, when a SNR is struck from the outside, it may not be necessary to break through a uniform shell as thick as that suggested by ΔR in Table 1. The above instability develops from small perturbations in the shell, but one in fact expects large perturbations to be present in SNR shells. When a dense shell forms behind the spherical shock front of an isolated SNR, the shock speed drops suddenly and the cooling gas following the shock is strongly decelerated as it runs into the slowing shell. It is very likely that a Rayleigh-Taylor instability grows at this stage (Kahn 1975). If the preshock medium is cloudy, the instability takes on the character of the Chevalier-Theys mechanism. Unfortunately the magnetic field topology has an important influence on the detailed nature of the instability. The dynamical effects of tangled and uniform fields in the shell are compared briefly by Chevalier (1974). Nonuniformities in isolated SNR shells also arise after about 10^6 yrs in a uniform interstellar field because flux tubes bent by the SNR expansion tend to straighten and move toward the explosion center on a time scale given roughly by the radius of curvature of a bent flux tube divided by the Alfven speed in the tube.

Clearly the corrugated, filamentary, or fragmentary shells resulting from the preceding processes will develop low-density connection channels more quickly than uniform shells when struck by strong shocks. SNR cavity connec-

tions seem virtually assured, although a proof by hydrodynamical calculation has only been attempted by Jones (1975a), whose computer code was inadequate to provide a conclusive test.

IV. EVOLUTION OF MULTIPLE CAVITIES

A well established chain or cluster of cavities is similar to an isolated cavity in having hot, low-density gas which is cooling slowly and low magnetic field strength. The boundaries or "walls" of the cavity are composed of portions of old shells of component SNRs and, in part, of clouds or "inclusions" which were enveloped by SNR shock fronts or have migrated into the cavity. The hot cavity gas reacts to at least three processes: 1) Distortion and spatial redistribution by interstellar motions (CS), 2) cooling and thermal conduction, and 3) sporadic reheating and repressurization above P_{ISM} by fast shock waves reverberating through the cavity. Consider the third process.

a) Shock Waves in Tunnels

When a strongly expanding SNR intersects a chain (if it is very long we may call it a "tunnel"), it may eventually initiate a strong shock wave in the low-density gas, promptly for inside SNe and after some delay for outside SNe. In one likely topology, tunnels may be considered as having low-density branches leading away from the locality of the intersection, so that the shock divides into "tunnel shocks" into various branches and "wall shocks" into high-density matter. The

wall shocks involve more and more wall surface as the faster tunnel shocks advance.

The shock fronts generated in a tunnel by one supernova, along with their enclosed volume, will be called a shock system. Figure 1 shows a simple shock system involving a cylindrical tunnel. The rate of change of the volume of this shock system is

$$\frac{dV}{dt} = 2 A v_{st} + S v_w \tag{7}$$

where A is the cross-sectional area of a branch of the tunnel undisturbed by the new shock system, S is the wall surface area already affected by the system, and the factor of 2 refers to the two branches in Figure 1. The tunnel shock speed v_{st} and the wall expansion speed v_w are derived in the Appendix, and their different character is related to the different sorts of pressure jumps at tunnel shocks and wall system boundaries. Tunnel shocks are approximated by pressure waves with a jump $P_2 - P_1$, where P_1 refers to the unshocked tunnel and P_2 to the shock system. When P_1 is comparable to P_2, it does not cost much energy to rejuvenate the tunnel gas, and the tunnel shocks may be weak although they are still fast. One may assume that tunnel shocks add volume and perhaps some energy (from P_1) to the system without doing much work. However, the wall expansion constitutes an essentially adiabatic movement against P_{ISM} which does work, the work appearing as power radiated behind the slow shock. Therefore

$$\frac{dP_2}{dt} = -\frac{1}{V}\left[(P_2 - P_1)\,2\,A\,v_{st} + \frac{5}{3}\,P_2\,S\,v_w\right] . \qquad (8)$$

Dividing (8) by (7) yields an equation for dP_2 / dV which has two simple limiting solutions: In the early phase of a shock system v_{st} is large, $P_2 >> P_1$, and A is still comparable to S. Then one can neglect terms like Sv_w and find $P_2 \propto V^{-1}$. But after a time, Sv_w becomes larger than Av_{st}, and volume is being added to the shock system by wall expansion much more rapidly than by tunnel shock propagation. Then $P_2 \propto V^{-5/3}$ until it approaches P_{ISM} and levels off because $v_w \rightarrow c_s$, the sound speed in the walls. In a tunnel of arbitrary geometry the terms containing A should be replaced by a sum over all the branches of the tunnel, but a time is usually reached for a strong shock system when wall expansion dominates dP_2 / dV.

b) An Example

It is appropriate now to present an example of SNR connection and of a two-remnant or binary shock system. For convenience the example will be discussed within the framework of the computer simulation, which is not described until the next section, and the opportunity is taken to suggest the modest level of accuracy with which a simulation can represent physical processes. Consider the representative evolution of a pair of SNRs shown in Figure 2. The second one occurs nine 50,000-year time steps after the first and 60 pc away. The pressures and radii would roughly follow Table 1 until both the interaction and the connection delay $t_{cross} + t_{R-T}$ have occurred. In Figure 2 this delay

begins at the "intersection" time t_{int} and lasts until the "connection" time t_{con}. After t_{con}, P_i must drop on the average more rapidly than in the isolated remnant evolution, due to simultaneous expansion of the shock system into the old cavity and spherically. To ensure that the time-averaged system pressure is not overestimated in the simulation where the actual hydrodynamics are not done explicitly, the two pressure drops are calculated separately. On each time step after t_{con}, a trial integration is performed of the pressure drop ΔP_{cav} which would occur if the shock had started across the old cavity at t_{con} driven by the current $P_2 = P_i$ of the shock system. The current P_2 is lower than at t_{con}, because the new SNR continues to evolve normally. The trial propagation beginning at t_{con} has a duration Δt_{prop} (which in the particular case of Figure 2 is larger than a time step). If the result of the trial indicates that the propagation would be at least half over within the current time step, then the cavity shock takes effect as if it occurred instantaneously at this time, t_{cav}. Otherwise the only drop in P_2 for that step is due to normal spherical expansion (if a binary system, or adiabatic wall expansion over the current surface area S if the system already covers more than one SNR). At the chosen t_{cav}, the pressure drop ΔP_{cav} is well approximated by the result of the calculation shown by the dashed line in Figure 2a. ΔP_{cav} is subtracted from P_2, which thereafter describes the pressure of both cavities, since pressure equilibrium is roughly maintained throughout a shock system (see Appendix). The compression of cavity shock propagation into a single time step is required by the simulation,

since there is no way to represent the position of a shock which has crossed a cavity partially; see §V. The final linear increase in radii in Figure 2b is due to the relaxation of P_2 to P_{ISM} by expansion over the wall surface S as mentioned above.

Note that the most effective shock systems for rejuvenating tunnels are actually initiated by SNe within a cavity rather than outside as in the example above. In such stronger shock systems, of which Figure 1 is a contrived example, there is no connection delay and the first cavity shock is completed when P_2 is still quite high, perhaps enabling several cavities to be shocked in quick succession.

c) Lifetimes of Tunnels

The rejuvenating influence of shocks on the cavities they pass through has been demonstrated in §§II and III. Here it may be added that for two cavities connected by a previous binary interaction, a later tunnel shock tends to reopen the low-density channels that form the essential connection: A shock compresses inclusions which clog the channels, and the divergence of the shocks leaving the connection tends to move the walls away from the channels if the Chevalier-Theys mechanism is operative.

A small amount of reheating of the cavity gas every few million years keeps ahead of radiative cooling. Thermal conduction in a very old section of tunnel could become important if the heat exchange area perpendicular to the field

increases substantially with time. Otherwise equation (5) tells us that the replenishment of 2×10^{49} ergs every 19/N million years years to each unit cavity volume ($\sim 10^{61}$ cm^3) keeps ahead of conduction. If the effect of both cooling and conduction is to decrease the cavity pressure below P_{ISM} , a shock repressurization to, say, 10% above P_{ISM} both pays the energy debt and forestalls the collapse of the cavity. Such a repressurization is quite easily supplied by tunnel shocks in the models to be discussed. Most tunnel shocks provide at least 1.3 P_{ISM}.

Of course if rejuvenating shocks fail to appear for τ_{SNR}, equation (1), the channels and tunnels may become clogged. If a cavity is allowed to cool, it is probably first filled by intercloud gas at 10^{3-4} K from evaporation of clouds by the ultraviolet flux of hot stars which will be free in cavities; cf. Elmergreen (1976). But many regions survive through rejuvenation so long that they are removed from the disk principally by buoyancy as discussed by Jones (1973). This process will not be considered in detail in this paper, but it should be remembered that the buoyant force on a hot "bubble" is zero at the midplane and increases with height as long as the Z-component of the galactic gravity increases. Therefore at the midplane where the SN rate per unit volume is highest and tunnels are most prevalent, buoyancy is weak.

V. METHOD OF SIMULATION

Model SNe are distributed randomly in space and time throughout a test volume representing a square section through the gaseous galactic disk in a spiral arm in the solar neighborhood. As time passes one must calculate and maintain information about the lifetimes, intersections, and shock systems of the collection of active and inactive living SNRs. Special care is needed to make conservative estimates of imperfectly understood phenomena and the somewhat arbitrary parameters that arise in the equations; where errors are likely, we have tried to err on the side that minimizes tunnel growth.

If a numerical experiment is to be meaningful, it is necessary to specify carefully which of the possible experiments has been performed. Several aspects of the simulation should be mentioned at the outset. First, cavities are spherical, being represented by a birth location and time and by a radius R_i. However, a calculational method has been found to allow for tangled or cloudy tunnel structure when propagating tunnel shocks. Secondly, no mass motions of the gas are followed explicitly. Motions are implicitly treated in the models already described for evolution of isolated remnants and propagation of shocks in chains of cavities. Thirdly, SNRs can occur only on the mesh points (spacing 10 pc) and time steps (50,000 yrs). The resulting granularity is small compared with significant distances and time scales for SNRs and is on the order of uncertainties which are generated by subsequent manipulations of SNRs present in the test space.

The simplest version of the simulation which has been investigated assumes that SNRs expand instantaneously to a radius of 40 pc, that any two overlapping living SNRs instantly make a perfect connection, and that one new intersection with a chain of remnants instantly rejuvenates the entire chain, no matter how long. With these unreasonable assumptions, the growth of a tunnel system depends solely on the value of the porosity q, equation (6). However, for porosities so low that tunnels did not grow, they cannot grow for any assumptions. The results indicate q must be greater than about 0.01, whereas galactic SNRs certainly amount to more than this. The second version of the simulation, the results of which were quoted in CS, contained a considerably more realistic treatment, but there were errors and unnecessary assumptions which have been corrected in the version described in this paper. Smith (1975) describes these differences in detail, but from now on only the latest version will be considered.

The size of the space represented was $X \times Y \times Z = 400 \times 400 \times 250$ pc^3. In order to prevent spurious surface effects at the artificial X and Y boundaries, repeating boundary conditions were imposed to mimic the behavior of the larger galactic disk; this means for example that an expanding SNR having a center at low enough X (or Y) can expand across the boundary and make a connection with a SNR at high X(or Y). In contrast, surface effects on the top and bottom of the test space will occur and must be allowed, because the thickness of the real disk is not much larger than the SNR diameter. Remnants near these boundaries are allowed to expand into the volume above the test space, representing a galactic halo, although no SNe occur outside the space.

The Z-distributions of SNe and gas have not been treated comprehensively at this stage of the work. That of SNe has been included, but the gas distribution is modeled by the disk with constant density n_0 sandwiched between two halo atmospheres with a lower constant density n_H . High-altitude SNRs will interact with the hot, flattened halo which various authors have proposed and which is predicted on the basis of the CS model. Such a halo is supplied with hot diffuse gas by convection from the disk, e.g. Jones (1973) and with mechanical energy by shock waves of high-altitude SNRs, e.g. Chevalier and Gardner (1974). The SN distribution in Z was taken to be a decreasing exponential with scale height 90 pc, symmetric about the center of the test space (Z = 0) as proposed by Hovaisky and Lequeux (1972). This distribution is applied here only out to Z = 120 pc where it is effectively truncated. Higher-altitude SNRs will affect only the halo, whereas we are primarily interested in the disk.

In the time steps following the birth of each SNR, it was expanded according to Table 1. If a SN occurred within an existing cavity, its entire blast energy was available to begin a shock system. This approximation is not too bad since the time scale for radiation is longer for an explosion in a lower density (Chevalier 1974). Lower fractions of E_0 are available for systems resulting from intersections made only after some expansion. For increased resolution during a remnant's initial step when almost half the expansion takes place, this step was divided in half as indicated in Table 1. To remain conservative in the matter of connections, an overlap of the spheres of radii R_i of two SNRs was required

to initiate a connection, rather than an overlap of one shock radius R_s and one inner cavity radius R_i. If the calculated delay $t_{cross} + t_{R-T}$ found at t_{int} was so long for an intersecting pair that negligible pressure would have been available after the delay had elapsed, the connection was rejected and the two SNRs remained unlinked. In the borderline case, a viable connection was made but the older SNR was not rejuvenated; a later shock system could propagate through such a connection.

Shock systems arising from SNe in cavities and from successful connections were expanded by the method of §IV. In doing this, it was necessary that the entire volume ΔV of a SNR which is added to the system be shocked in one uninterrupted procedure; otherwise the shock fronts would normally have been left delineating partial SNR volumes, and some further specification of the spatial extent of SNRs would have been necessary beyond their centers and radii. The maintenance of identifiable component SNRs in a chain is a weakness of the method but is also what makes it feasible. In complex situations where a shock system simultaneously expands into branches with fast local tunnel shock speeds and branches with slow speeds, the order in time of cavity shocks and pressure drops was carefully observed.

The tunnel shock area A in equations (7) and (8) was evaluated in the geometry of intersecting spheres. The value of S to be used is a more important quantity, since wall shocks predominate for most of the duration of a system. One might continue to visualize a tunnel as a set of overlapping spheres, but

this would seriously underestimate the surface-to-volume ratio S/V which a region presents to a propagating shock system. In the computer code, old tunnels appear tangled on dimensions smaller than isolated SNR sizes, i.e. similar to embedded cloud sizes, in spite of the restricted spatial information, by letting each SNR have an S/V $\equiv \eta$ which increases with time t after the SN blast time t_{SN} according to the law

$$\eta(t) = \eta_f + (\eta_i - \eta_f) \exp\left(-\frac{t - t_{SN}}{\tau_{SV}}\right) \tag{9}$$

Here the initial ratio is that of a cylinder of radius 30 pc, i.e. $\eta_i = 0.067$ pc^{-1}, while the final ratio attained is that of a cylinder of radius 5 pc, i.e. $\eta_f = 0.4$ pc^{-1}. The age of the SNR, $t - t_{SN}$, may be many isolated remnant lifetimes. The time constant τ_{SV} has been given the value 4×10^6 yrs to agree with the lifetime hypothesis. Almost any tangling assumption has an enormous effect on the distance a shock system can extend in an old section of tunnel. To obtain ΔS swept into the shock system, as a volume ΔV is swept out, one calculates $\Delta S = \eta(t)\ \Delta V$, using η for the SNR into which the shock propagates.

SNe occurring within 30 pc of the test space boundaries in the Z-direction (the top and bottom three layers of mesh points) were assumed to make "connections" with the diffuse halo whether or not connections were made with other SNRs. In keeping with the assumption of uniform density, a halo-connected SNR which became part of a shock system was assumed to be the center of a

hemispherical halo shock front which began after the shock system had rejuvenated the SNR and continued with increasing radius into the halo, contributing to the drain on shock system pressure until $P_2 \rightarrow P_{ISM}$. A more accurate treatment might consider the actual gas distribution at high Z and the non-spherical nature of high-altitude SNRs (Chevalier and Gardner 1974). The halo shock speed was given by equation (A.5) using $P_H = 8 \times 10^{-13}$ dyn cm^{-2} instead of P_1 and $\rho_H = 6 \times 10^{-27}$ g cm^{-3} instead of ρ_1 ; these values are suggested by models of a halo arising from hot material welling up from the tunnels (Cox 1974; cf. Spitzer 1956) or from accretion of local intergalactic matter (e.g. Cox and Smith 1976). This very approximate view of the disk and halo can be compared with theoretical models of the Z-distribution of matter such as Kellman's (1972). However, the aim here was simply to include some representation of the existing sink for high-altitude SN energy and avoid its spurious concentration to the disk.

If a shock system managed to shock all the SNRs in a short chain or cluster before depressurization to P_{ISM}, it was then allowed to continue pushing out its walls until equilibrium with P_{ISM} was reached. This adiabatic expansion affects only the outer walls and not the inclusions. Thus the surface S used in integrating (7) and (8) for this purpose is just the outer boundary of some configuration of overlapping spheres. The expansion produces a ΔR_i during one time step which is added to each R_i in the system, and can increase R_i above $R_{if} = 46.7$ pc. An arbitrary upper limit of 60 pc was placed on R_i , because

without buoyancy one remnant could expand to fill the test volume, an unrealistic situation which would be an artifact of the assumption that SNRs retain their identity within a chain.

The rejuvenation of a SNR by a shock system was accomplished by revising its projected death time from $t_{SN} + \tau_{SNR}$ (or its most recent value) to equal that of the SNR which initiated the rejuvenating shock system. However, its life expectancy was never reduced thereby. This estimate of the degree of rejuvenation reflects the fact that an older shock system cannot extend a SNR's lifetime as much as a newer system, but as mentioned previously the exact amount of the extension must be regarded as unknown. Since the degree of rejuvenation is a critical consideration, one comparison run with a high SN rate was made in which a remnant's death time could be extended upon rejuvenation by only half the above amount. As discussed in the next section, the fraction of the whole test volume ending up in tunnels was somewhat lowered by this change.

At the end of each time step, all isolated SNR that had lived to their limit were totally erased from the test space, and their positions effectively restored to uniform n_0 wherever living remnants did not extend. All chains that had one or more members due to die were analyzed to erase only those SNRs which were too old; members do not have the same death time unless they were most recently rejuvenated by the same shock system. For example, if a long, straight chain were very old when it was intersected by new SNRs at both ends, the

middle of the chain might die and be erased before the two shock systems met, leaving two pieces no longer having a connection.

Considerably more detailed simulations can certainly be imagined, but for generalized chains even this approximate formulation is already rather complicated to encode for the computer.

VI. RESULTS AND DISCUSSIONS

Results will now be presented for a sequence of simulations having the same values of E_0 , n_0 , and τ_{SNR}, but different SN rates per unit volume, r. Table 2 lists the parameters used in the various runs. The fraction $\langle f \rangle$ of the test volume contained in SNR cavities (angle brackets denote averages over Z) is the most basic calculated quantity and as used in the following includes both isolated and connected SNRs. To give the reader a feeling for the fluctuations in $\langle f \rangle$ for different r, $\langle f \rangle$ is plotted in Figure 3 as a function of time for the runs, along with the "random input function." The same random set (taken from Rand 1955) has been used for all runs, merely varying the rate at which SNe are put into the space, so that in each run they appear at the same positions and in the same order and relative spacing in time. Although the runs are short, the poor statistics are compensated by the clarity with which the effect of varying r can be isolated. To test for bias of the common data set, which would affect all runs, two additional data sets were compared for one rate. No bias tending to increase $\langle f \rangle$ was found.

Although the results depend separately on $<r>$, τ_{SNR}, and V_{SNR}, one may characterize the runs by their values of $<q>$ since only $<r>$ is varied. The exponential Z-distribution of SNe has been truncated in such a way that up to 26% of the total galactic SNe would fall outside the space, depending on how far the distribution holds. Thus in Table 2 the Z-averaged r is given for each model, and the equivalent galactic rates are derived for truncation at Z = 120 pc and $Z = \infty$.

Let us now focus individually on the types of results obtainable from this study.

a) Death and Rejuvenation of Remnants

Table 3 presents the distributions of SNR ages in the form of percentages of SNRs with ages in the ranges given in the first column. Only SNRs which died by the end of the run are included. The average age at death increases steadily with $<q>$ for the sequence of Models A, B, and C. In fact, a short run performed for $<q> = 0.30$, which is not shown in Figure 3, gave an average age more than twice as long as τ_{SNR}. These average values appear on Figure 3 as " τ_{eff} ."

b) Shock Waves in Tunnels

Tables 4a and b give the distributions of peak cavity shock speed v_{st} (e.g. at the highest point on the dashed line in Figure 2a) and of the peak wall speed v_w, for each unit cavity which was crossed by a shock system throughout the

run. During Δt_{prop} both speeds drop. The v_{st} distribution is peaked at c_s but has a second maximum at the high end due to strong shocks from SNe within cavities, and the v_w histograms have a similar structure.

In Table 4c are propagation times Δt_{prop} for the same sample of shocks. The breadth of the distributions, which cover an order of magnitude, is due to differences in Δt_{prop} between fast v_{st}'s across small cavity volumes ΔV and slow v_{st}'s across large ΔV's.

c) Fraction of Interstellar Volume within Tunnels

The duration in time represented by the runs in Table 2 and Figure 3 is about 15 $<q>^{-1}$ Myrs. Within this time each run attained a quasi-steady state in which $<f>$ averaged more than $<q>$. If SNRs enjoyed no cooperative interactions, one would obtain $<f> = 1 - e^{-<q>}$. Here it is apparent that the extension of SNR lifetimes through rejuvenation has added more cavity volume than has been lost from the incomplete expansion of SNRs which break into other cavities.

The quantity $<f>$ averaged over time, $<\bar{f}>$, is plotted in Figure 4 against $<q>$ with approximate uncertainties in the quasi-steady value estimated from Figure 3. Models A, B, and C are barely consistent with a straight line through the origin, although a better fit is given by a function which is concave upward. Figure 4 includes the run at $<q> = 0.30$ mentioned previously.

The critical value of q, which CS implied would separate slow tunnel growth from rapid and extensive growth, was not found here for $<q> \leq 0.30$,

i.e. SN rates $\lesssim$ (25 yr gal)$^{-1}$. The tendency of all runs to reach a quasi-steady $<f>$ does not encourage a search at higher q for such a critical value. However, by performing very long runs one might detect a critical q-dependence for a secular increase in $<f>$ above these quasi-steady levels.

A general property of tunnel growth in these runs, which summarizes the results so far and explains the lack of critical behavior, will now be discussed: Tunnels are primarily built and enlarged by intersections between very old SNRs and new ones in the Sedov phase, but once tunnels develop they are kept rejuvenated by SNe occurring within their volume. Isolated SNRs spend most of their time fully expanded, and a matrix of binary interactions like the example in §IVb shows that such old SNRs with thick shells ($R_{if} \simeq 47$ pc, $\Delta R \sim 13$ pc) are hard to rejuvenate. It can be done by a SN inside the cavity or by one outside but still in the Sedov phase, $R_i \lesssim 24$ pc, when it intersects. The probability that a SN will occur within a distance R of a very old SNR within its lifetime is $p_{out} = 1 - e^{-\alpha q}$, where $\alpha = (R_{if} + R)^3/R_{if}^3$. In CS we claimed that $R = R_{if}$ would produce a connection, i.e. $\alpha = 8$. From the requirement that the active SNR be in the Sedov phase we find $\alpha \simeq 3.5$. For $<q> = .25$, the mean probability for being rejuvenated once by an outside SN is thus .63, but the weak shock system usually stops after the single SNR. On the other hand, with $<q> = .25$ there is a fairly high SN rate within the tunnels themselves, each SN capable of rejuvenating $V_t \simeq 2 \times 10^{62}$ cm^3 (CS), i.e. to a distance $R_t \sim 200$ pc, if such a fully connected tunnel network has been built

that V_t is available. Once rejuvenated at some time, the volume is guaranteed a second rejuvenation by another occurrence within a time $\tau_{SNR} - t_{prop}$ (where $t_{prop} = \Sigma \Delta t_{prop}$ for the chain). Since the average tunnel shock speed for Model C was about 350 km s^{-1}, one estimates $t_{prop} \sim R_t/v_{st} \sim 0.6$ Myr. Hence the probability of rejuvenating V_t is $p_{in} \simeq 1 - \exp\ [-r(\tau_{SNR} - t_{prop})V_t] \sim .97$, in an extensive tunnel network. But SNRs originating within tunnels add little or no volume to the tunnel. The comparison of p_{out} and p_{in} emphasizes the connection-damping effect of SNR shells.

d) Z-Distribution of Volume Fraction

Figure 5 shows a typical relationship, at the end of Model B, between the distribution of SNe with height above the plane, represented here by q(Z), and the resultant fraction f(Z) of the volume left in tunnels and SNRs. The values of f(Z) for positive and negative displacements from Z = 0 have been averaged together; the breadth of the low-Z peak is a measure of the fluctuation in the position of the maximum f(Z) around Z = 0, roughly ±20 pc. At high Z we see that $f(Z) \sim q(Z)$ in agreement with the low effective porosity there and the low probability for SNR interaction. The curves for f(Z) and q(Z) separate near Z = 100 pc, and f(Z) substantially exceeds q(Z) near the midplane. The SN rate per unit volume there is ~ 1.7 times the Z-averaged rate, which causes tunnels to grow first in this vicinity. Over a very long time they might spread to higher Z, which would provide a secular increase in the average $\langle f \rangle$.

For all four runs, the relation of f(0) to q(0) is almost the same as that between $\langle f \rangle$ and $\langle q \rangle$ in Figure 4.

The f(Z) vs. Z curve should become flatter for a model in which both the scale height of ambient gas and the density decrease with Z are taken into account, because SNRs with the same E_0 will reach larger R_{if} in lower n_0. In fact it is possible that a correct treatment of high-Z SNRs with the same Z-distribution used here would show f(Z) increasing with height, a question which deserves further study: The slope of f(Z) vs. Z depends critically on the competition between the scale heights of the gas and SN distributions, as suggested by Reynolds (1975). The interaction between tunnels and the galactic halo ultimately depends on similar considerations. The eventual outcome of the development of high-altitude tunnels is the expulsion of hot gas from the galactic disk (cf. Paper I, Spitzer 1956, Jones 1973, Shapiro and Field 1976).

e) Radii of SNR Cavities

In these simulation models the radius of a SNR depends on its history in spite of the fact that all begin identically. A very young remnant that drives a shock into a neighboring cavity is rapidly depressurized and may not reach its full radius; after t_{int} in such a case the remnant expands until t_{cav} when the first cavity is actually "shocked."* Furthermore, a SNR whose expansion has ceased may renew it if subsequently repressurized, unless $R_i = 60$ pc.

With these aspects of the simulation in mind we present the distributions of radii observed for the runs in Table 5. The average SNR radius is less than

*Without including this expansion after intersection it is possible to find parameters for which the simulation gives $f < q$ due to strong quenching of SNR expansion.

roughly R_{if} for all runs and decreases with increasing q. A similar decrease is observed for the average radius at intersection. A comparison of Tables 5b and c shows the substantial increases of R_i between t_{int} and t_{cav}.

The results for the radii when one takes a snapshot of the test space at a typical time may be summarized very roughly by constructing graphs of the number of SNRs with diameter D_i less than a certain value. A set of such curves, each averaged over a run, is given in Figure 6. On the time scale of the simulation, millions of years, there are never an appreciable number of remnants with $D_i < 50$ pc. The simulation does not need to resolve such small diameters, since the evolution of SNRs at this stage is mostly unaffected by interactions. Most SNRs predicted by these runs will be larger and luminous in soft X-rays, not radio emission, because a cavity cooling time is required for the decay of the X-ray emission (cf. Naranan, et al. 1976), whereas the radio emission decays quickly into the background continuum. The soft X-ray background excess is probably a SNR superposition of some sort, but SNRs cannot be distinguished individually nearly as far in X-rays as in radio emission because of absorption, so that we cannot begin to construct a catalog of large galactic SNRs. Nonetheless, it is interesting to compare in Figure 6 the curve of Clark and Caswell (1976) for radio SNRs. Several features of these curves viewed together are evident: First, the "radio" and "X-ray" curves have essentially no overlap; the turnover in the radio curve above D = 35 pc is probably a limiting-surface-brightness effect. Secondly, large-diameter SNRs in the runs,

D_i = 50 - 100 pc, have $N(<D_i)$ curves which are always steeper in general trend than the approximate D_i^4 proportionality expected for "momentum- conserving" SNRs which have formed dense shells. This can be understood as incomplete expansion of interacting SNRs; many SNRs have smaller diameters on the average than would be expected if all expanded independently. This steepening is most evident for D_i = 50 - 70 pc in Model C. Thirdly, if one scales the number of SNRs in the 400 × 400 pc^2 test space by the total area of the disk, accounting for a nonuniform SN rate over the disk, one finds a plausible correspondence between the predicted radio and X-ray curves, e.g. as shown by the dashed line extrapolation in Figure 6. For this line, chosen arbitrarily to be determined by Model B at large D_i, a scale factor of 10^3 was assumed, which would make sense if one third of the galactic disk (R = 12 kpc) were subjected to a rate per unit volume equivalent to a uniform galactic rate of $(40 - 50\ yr)^{-1}$. Maza and Van den Bergh (1976) have recently confirmed that SNe seem to be somewhat concentrated to spiral arms. Also, Ogelman and Maran (1975) have proposed that young stellar associations are sites of multiple, correlated SN explosions. Because of this possible clustering and because the growth of tunnels depends on the SN rate per unit volume, the above steepening may occur even with an average galactic rate as low as the $(150\ yr)^{-1}$ favored by Clark and Caswell. There is a hint of steepening in their radio $N(<D)$ curve for D = 30 - 35 pc which could possibly correspond to the steepening predicted by the tunnel model. It would then be predicted that the thousands of soft-X-ray-emitting

SNRs in the Galaxy should show a steep $N(<D_l)$ curve in intermediate diameters, although it is not clear how many can be observed. Seward, et al. (1976) have compared radio and X-ray fluxes from SNRs and find that many are unexpectedly faint in X-rays. However the larger distance scale adopted by Clark and Caswell leads to many disagreements with Seward, et al. on the distances and diameters of SNRs and tends to weaken this conclusion.

f) Effective Remnant Volumes

The volume of a SNR that remains isolated is simply $V_{SNR} = 4.3 \times 10^5$ pc^3, but if it initiates a shock system, then its effective volume is the eventual volume of that system. Both cases are included in Table 6 which lists V_{eff} for SNRs which died and for shock systems which were erased by the end of each run. A broad range of values is found, particularly for the higher SN rates. Note the high values in the second bin indicating that a common class of shock systems propagate through only about one cavity or twice V_{SNR}, in agreement with the discussion at the end of §VIc.

VII. CONCLUDING REMARKS

Dense, thick shells insulating SNR cavities provide effective damping on the rate of remnant connections, but they by no means prevent all SNR interactions. Remnants of 6×10^{50} erg explosions can break through shells $\gtrsim 10$ pc thick if they begin while still in the Sedov phase, because a Rayleigh-Taylor

instability occurs which is enhanced by irregularities in the shell. SNRs which occur outside in relatively dense locations and break into a tunnel add volume to the tunnel network but initiate only weak shock systems, while SNe which occur inside tunnels add no volume (taking the shape of their surroundings) but create very strong shock systems. Lifetimes of cavities, both single and multiple, probably depend chiefly on magnetic field topology over scales smaller than a remnant, since thermal conduction cooling depends sensitively on field geometry and radiative cooling does not destroy cavities.

Numerous assumptions must be made to make progress on a global simulation. The resulting tunnel filling fraction is strongly influenced by sizes of isolated SNRs, which depend in turn on the choice of E_0, n_0, and the point at which expansion is halted ($P_i \rightarrow P_{ISM}$). Cloudy inclusions within tunnels can be accounted for roughly by using a growing surface-to-volume ratio for each SNR cavity. The combination of a uniform density disk, sandwiched between uniform lower-density haloes, with a realistic Z-distribution of (identical) SNRs gives tunnel filling fractions which fall off with Z. Within this conceptual framework the numbers of effectively free parameters is understandably high, and the parameter space has not been exhaustively explored. However, fixing one's choices for most of them, the dependence on the SN rate per unit volume as independent variable can be understood. For the life and death of the population of galactic SNRs as a whole the chief dependences are on V_{SNR}, τ_{SNR}, and the degree of rejuvenation resulting from shocks which propagate through a

cavity. Critical growth of the tunnel filling fraction f for certain minimum values of porosity q (CS) was not found here, but rather a quasi-equilibrium in which $f \gtrsim q$. The quenching of SNR expansion by early interactions was found to be less effective than claimed by CS and by Jones (1975b).

The presence of a local tunnel network in some region, e.g. the solar neighborhood, depends on the SN rate per unit volume in that vicinity over the preceding 10^7 yrs, which may easily exceed the galactic average. SNe are concentrated at low Z (e.g. Clark and Caswell 1976), near spiral arms (Maza and Van den Bergh 1976), and perhaps near each other (Ogelman and Maran 1976). With respect to spiral structure, the density wave theory predicts passage through an arm in $\sim 10^8$ yrs, so that tunnels may be quickly established there and then decay in the interarm region. If galactic shocks are suppressed in a 10^6 K gas with high sound speed, various observations may require this interarm tunnel decay (Chevalier 1976). Soft X-ray spectral studies (Burstein 1976, Naranan, et al. 1976, Levine, et al. 1976) are still unable to prove a thermal origin for the emission* or to detect whether the solar system is near to or surrounded by hot SNR cavities which could account for all the observed soft X-ray background excess.

We do not accept the narrow view of Clark and Caswell (1976) that all galactic SNRs are known, because SNRs should be X-ray emitters long after

*Since the emission from tunnels is overwhelmingly collisionally excited lines (Kato 1976, Raymond, Smith, and Cox 1976, Shapiro and Moore 1976), the resolution of soft X-ray lines would be decisive.

they cease to be bright radio objects. But if their radio results are a good indication of present SN properties such as E_0, n_0, and the SN rate, then the structure of very hot interstellar regions may differ from the visualization of the present paper, which is based on earlier studies. Clark and Caswell find a ratio $E_0/n_0 \sim 5 \times 10^{51}$ erg cm^3 and a mean interval between SNe of $\lesssim 150$ yrs, both numbers being larger than found by earlier workers (e. g. Ilovaisky and Lequeux 1972). The final radii of such SNRs would be very large, and a relatively small number of such SNRs may in fact constitute sufficient cavity volume to explain the soft X-ray background excess, as suggested by Naranan, et al. (1976). In this case the porosity may still be large and SNR interactions thus frequent, but the scale of cavities is much larger compared to the thickness of the gaseous disk than in the models discussed in this paper. Interactions between SNRs would then assume less importance while those between SNRs and the galactic halo might determine the structure of hot interstellar regions, making fewer and generally wider cavities, rather than narrower but extensive tunnels.

It is a pleasure to thank my thesis advisor, Don Cox, for introducing me to this problem and for much guidance. Helpful suggestions were made by Roger Chevalier, Eric Jones, John Raymond, and Len Fisk. I am grateful to W. L. Kraushaar and B. D. Savage for interest and support. This research was supported in part by the Graduate School of the University of Wisconsin-Madison and NASA Grant NGL 50 - 002 - 044. Thanks are due to a number of

folks at the Laboratory for High Energy Astrophysics, where the manuscript was prepared while the author was a NAS-NRC Resident Research Associate.

APPENDIX

Shock system expansion into tunnels and walls is of different character, as one can discover from the expansion speeds. The equations of conservation of mass, momentum, and energy across a shock front are

$$\rho_1 v_1 = \rho_2 v_2 \tag{A.1}$$

$$P_1 + \rho_1 v_1^2 = P_2 + \rho_2 v_2^2 \tag{A.2}$$

$$5kT_1 + \frac{1}{2}mv_1^2 + \frac{B_1^2}{8\pi n_1} = 5kT_2 + \frac{1}{2}mv_2^2 + \frac{B_2^2}{8\pi n_2} \tag{A.3}$$

where ρ is the mass density and m is the mass of an average nucleus. For tunnel shocks one notes that the magnetic field is negligible in tunnels, so that the equations yield a compression factor

$$x = \frac{\rho_2}{\rho_1} = \frac{4P_2 + P_1}{P_2 + 4P_1} \tag{A.4}$$

and a shock speed

$$v_{st} = \left(\frac{4}{3}\frac{P_2 + \frac{1}{4}P_1}{\rho_1}\right)^{1/2}. \tag{A.5}$$

Immediately after a SN within a tunnel the program might have $P_1 \sim P_{ISM}$ and $P_2 \sim 430\ P_{ISM}$, resulting in $v_{st} > 1500$ km s^{-1} with $\rho_1 = 2 \times 10^{-26}$ g cm^{-3}. More typical speeds are five to ten times lower (§VI). As the expansion of the shock system proceeds, P_2 rapidly decreases and v_{st} drops to the sound speed, $c_s \sim 90$ km s^{-1}. If P_1 is higher than P_{ISM} due to recent passage of a different shock system, v_{st} is somewhat increased.

At a shock front in the walls, the magnetic field $B_1 \sim x_s \cdot 3\mu G$ (where x_s is the residual shell compression) is compressed anew along with the gas. These shocks are much slower than tunnel shocks due to higher ρ_1, and radiative cooling is important just behind the

shock. Since $B_2 \propto x$ in equation (A.3), the wall shock compression

$$x_{sw} = \left(\frac{P_2}{P_{w1}}\right)^{1/2}, \tag{A.6}$$

where $P_{w1} = B_1^2/8\pi + P_{cr}$ is the sum of magnetic and cosmic ray pressures. The shock speed is

$$v_{sw} = v_1 = \left\{\frac{P_2}{\rho_w}\left[1 + \left(\frac{P_{B1}}{P_2}\right)^{1/2}\right]\right\}^{1/2}. \tag{A.7}$$

However, as shown in the inset of Figure 1, this is not the speed of the inner edge of a wall of the shock system, which is

$$\begin{aligned} v_w &= v_{sw}\left(1 - \frac{1}{x}\right) \\ &= \left\{\frac{P_2}{\rho_w}\left[1 + \left(\frac{P_{w1}}{P_2}\right)^{1/2}\right]\right\}^{1/2}\left[1 - \left(\frac{P_{w1}}{P_2}\right)^{1/2}\right]. \end{aligned} \tag{A.8}$$

For a mass density in the walls of $\rho_w = 3\times10^{-24}$ g cm^{-3}, and the above value of P_2, $v_{ws} \simeq 120$ km s^{-1}. The value of ρ_w reflects the typical value of x_s, about 2. Values of v_w have a lower limit of the Alfvén speed $v_A \sim 6$ km s^{-1}.

Because the diffuse tunnel gas is hot and has a high sound speed, the pressure in different parts of the shock system tends to equalize. Just behind a shock front the pressure will be higher than average; however, if one assumes a power law decrease in density behind the front and a velocity pattern which maintains this density structure, it can be shown (Cox 1974) that the kinetic energy per unit mass of the motion associated with a tunnel shock is less than one sixth of the thermal energy per unit mass of the material near the shock, for any ratio of preshock to postshock pressure P_1/P_2. Both kinetic energy and the driving pressure P_2 cause the shock to advance. Since the total energy content of the shock system is shared between kinetic and thermal energy, we overestimate P_2 somewhat by assuming that all

energy fed into the system is thermal and that the interior of the system is in pressure equilibrium. A workable approximation is to ignore the kinetic energy when calculating the decay of P_2, because the lower than true rate of system expansion computed without this kinetic energy is increased by the compensating effect of larger P_2.

REFERENCES

Brown, R. L., and Gould, R. J. 1970, Phys. Rev. D, 1, 2252.

Bunner, A. N., Coleman, P. L., Kraushaar, W. L., and McCammon, D. 1972, Ap. J., 172, L67.

Burstein, P. H. 1976, Thesis, University of Wisconsin-Madison.

Castor, J., McCray, R., and Weaver, R. 1975, Ap. J., 200, L107.

Chevalier, R. A. 1974, Ap. J., 188, 501.

_____1975, Ap. J., 200, 698.

_____1976, private communication.

Chevalier, R. A., and Gardner, J. 1974, Ap. J., 192, 457.

Chevalier, R. A., and Theys, J. C. 1975, Ap. J., 195, 53.

Clark, D. H., and Caswell, J. L. 1976, Mon. Not. R. astr. Soc., 174, 267.

Cowie, L. L. 1976, Thesis, Harvard University.

Cowie, L. L., and McKee, C. F. 1976, preprint.

Cox, D. P. 1972, Ap. J., 178, 159.

_____1974, unpublished.

Cox, D. P., and Smith, B. W. 1974, Ap. J., 189, L105 (CS).

_____1976, Ap. J., 203, 361.

Elmergreen, B. G. 1975, Ap. J., 198, L31.

_____1976, Ap. J., 205, 405.

Frieman, E. A. 1954, Ap. J., 120, 18.

Greisen, E. W. 1976, Ap. J., 203, 371.

Heiles, C. 1973, in Galactic and Radio Astronomy, IAU Symposium No. 60, ed. F. J. Kerr and S. C. Simonson.

Ilovaisky, S. A., and Lequeux, J. 1972, Astron, & Ap., 18, 169.

Jenkins, E. B., and Meloy, D. A. 1974, Ap. J., 193, L121.

Jones, E. M. 1973, Ap. J., 182, 559.

_____1975a, B. A. A. S., 6.

_____1975b, Ap. J., 201, 377.

Kahn, F. D. 1975, preprint.

Kato, T. 1976, Ap. J. Suppl., 30.

Kellman, S. A. 1972, Ap. J., 175, 353.

Kraushaar, W. L. 1973, unpublished.

Levine, A., Rappaport, S., Doxsey, R., and Jernigan, G. 1976, Ap. J. 205, 226.

Maza, J., and van den Bergh, S. 1976, Ap. J., 204, 519.

McCray, R. 1976, private communication.

McCray, R., Stein, R. F., and Kafatos, M. 1975, Ap. J., 196, 565.

McKee, C. F., and Cowie, L. L. 1975, Ap. J., 195, 715.

McKee, C. F., and Ostriker, J. P. 1975, B. A. A. S., 7, 419.

Naranan, S., Shulman, S., Friedman, H., and Fritz, G. 1976, preprint.

Ögelman, H. B., and Maran, S. P. 1975, preprint.

Rand Corporation 1955, A Million Random Digits (Glencoe, Illinois; Free Press).

Raymond, J. C., Cox, D. P., and Smith, B. W. 1976, Ap. J., 204, 290.

Reynolds, R. J. 1975, private communication.

Scott, J. S. 1975, Nature, 258, 58.

Seward, F., Burginyon, G., Grader, R., Hill, R., Palmieri, T., Stoering, P., and Toor, A. 1976, Ap. J., 205, 238.

Sgro, A. G. 1975, Ap. J., 197, 621.

Shapiro, P. R., and Field, G. B. 1976, Ap. J., 205, 762.

Shapiro, P. R., and Moore, R. T. 1976, Ap. J., in press.

Smith, B. W. 1975, Thesis, University of Wisconsin-Madison.

Snow, T. P., and Morton, D. C. 1976, preprint.

Spitzer, L. 1956, Ap. J., 124, 20.

_____1962, Physics of Fully Ionized Gases (New York: Interscience).

Spitzer, L., and Jenkins, E. B. 1976, Ann. Rev. Astron. & Ap., 13, 133.

Vanderhill, M. J., Borken, R. J., Bunner, A. N., Burstein, P. H., and Kraushaar, W. L. 1975, Ap. J., 197, L19.

Verschuur, G. L. 1974, in Galactic and Extra-Galactic Radio Astronomy (New York: Springer-Verlag), ed. G. L. Verschuur and K. I. Kellerman.

Williamson, F. O., Sanders, W. T., Kraushaar, W. L., McCammon, D., Borken, R., and Bunner, A. N. 1974, Ap. J., 193, L133.

York, D. G. 1974, Ap. J., 193, L127.

Table 1

Calculated SNR Evolution, $n_0 = .7\ cm^{-3}$, $E_0 = 6 \times 10^{50}$ ergs.

t_5 (yr)	R_s (pc)	v_s (km s^{-1})	$\frac{E_i}{E_0}$	<X>	ΔR (pc)	R_i (pc)	P_i (10^{-12} dyn cm^{-2})
.25	17.6	276	.72	4	0	17.6	430
.5	22.2	182	.63	4	0	22.2	190
1.0	28.2	84.3	.17	20	0.5	27.7	25
1.5	31.5	63.7	.088	14	0.8	30.7	10
2.0	34.5	52.3	.074	10	1.2	33.3	6.5
2.5	36.9	44.8	.063	8	1.6	35.3	4.7
3.0	39.1	39.5	.057	6	2.3	36.8	3.7
4.0	42.7	32.4	.048	4.0	3.9	38.8	2.7
5.0	45.8	27.8	.043	3.5	4.9	40.9	2.1
6.0	48.4	24.5	.040	3.0	6.0	42.4	1.7
7.0	50.8	22.0	.038	2.7	7.1	43.7	1.5
8.0	53.0	20.0	.036	2.5	8.2	44.7	1.3
10.0	56.8	17.2	.034	2.1	10.8	46.0	1.1
12.0	60.1	15.2	.033	1.9	13.3	46.8*	1.0

*Final cavity radius R_{if}.

Table 2

Parameters Used in the Runs

	Model			
	A	B	C	L*
$\langle q \rangle$, volume-averaged porosity	.15	.20	.25	.25
Volume-averaged SN rate within 120 pc of Z = 0 (yr^{-1} gal^{-1})	66^{-1}	50^{-1}	41^{-1}	41^{-1}
SN rate including high-Z SNe; rate for whole galaxy (yr^{-1} gal^{-1})	49^{-1}	37^{-1}	30^{-1}	30^{-1}
$\langle r \rangle$, SN rate per unit volume at $\lvert Z \rvert$ = 5 pc (10^{-7} Myr^{-1} pc^{-3})	1.5	2.0	2.4	2.4
Elapsed time (Myr)	98	69	52	59
SN blast energy E_0 (ergs)		6×10^{50}		
Ambient ion density n_0 (cm^{-3})		.7		
Isolated SNR lifetime τ_{SNR} (yr)		4×10^{6}		
Final isolated SNR volume V_{SNR} (pc^3)		4.3×10^{5}		
"Tangling" time constant τ_{SV} (yr)		4×10^{6}		
Tunnel ion density ρ_i (g cm^{-3})		2×10^{-26}		
Ambient interstellar pressure P_{ISM} (dyn cm^{-2})		1.0×10^{-12}		
Halo ion density ρ_H (g cm^{-3})		6×10^{-27}		
Halo pressure P_H (dyn cm^{-2})		8×10^{-13}		

*Half the rejuvenation lifetime extension of other runs; see §§III and V.

Table 3

Distributions of SNR Ages at Death

τ_{eff} Bin (Myr)	Model A	B	C	D
4 (%)	57	45	43	34
4 - 6 (%)	13	13	20	29
6 - 8 (%)	12	16	7	18
8 - 10 (%)	8	8	6	8
10 - 12 (%)	6	5	9	4
12 - 16 (%)	2	5	5	3
16 - 20 (%)	1	4	8	2
> 20 (%)	<1	3	3	<1
Average τ_{eff} (Myr)	5.8	7.2	7.5	6.4

Table 4

Distributions of Quantities for Cavity Shocks

Speed Bin ($km\ s^{-1}$)		Model A	B	C	D
a) PEAK TUNNEL SHOCK SPEEDS v_{st}					
$\leqslant 100$	(%)	13	12	14	14
100 – 200	(%)	54	54	54	56
200 – 300	(%)	8	10	12	9
300 – 400	(%)	2	4	3	4
400 – 600	(%)	3	3	3	3
600 – 1000	(%)	2	2	1	1
> 1000	(%)	18	15	14	13
Average v_{st} ($km\ s^{-1}$)		401	360	346	332
b) PEAK WALL EXPANSION SPEEDS v_w					
$\leqslant 15$	(%)	63	64	62	66
15 – 30	(%)	14	17	20	17
30 – 45	(%)	3	3	4	3
45 – 75	(%)	2	1	1	1
75 – 90	(%)	8	7	5	6
90 – 120	(%)	1	<1	1	<1
120 – 135	(%)	9	8	8	7
Average v_w ($km\ s^{-1}$)		31	28	27	26
c) SHOCK PROPAGATION TIMES Δt_{prop}					
Time Bin (10^5 yr)					
< 1	(%)	18	19	27	17
1 – 2	(%)	25	28	24	27
2 – 3	(%)	17	21	21	23
3 – 4	(%)	22	18	18	18
4 – 5	(%)	15	11	8	12
> 5	(%)	4	3	3	3
Average Δt_{prop} (10^5 yr)		2.6	2.4	2.2	2.4

Table 5

Distributions of SNR Radii

R_i Bin (pc)	Model A	B	C	D
a) RADII AT DEATH				
25 – 30 (%)	1	5	8	1
30 – 35 (%)	6	8	17	13
35 – 40 (%)	4	7	9	8
40 – 45 (%)	20	24	21	26
45 – 50 (%)	46	37	35	34
50 – 55 (%)	5	5	4	3
55 – 60 (%)	19	15	7	15
Average R_i at death (pc)	47	45	42	45
b) RADII OF ONLY SNRS WHICH MADE INTERSECTIONS, AT t_{int}				
0* (%)	31	33	41	36
17.6 (%)	31	29	27	33
22.2 (%)	7	8	7	6
27.7 (%)	10	10	8	10
30 – 35 (%)	13	14	12	11
35 – 40 (%)	8	6	4	4
> 40 (%)	0	0	0	0
Average R_i at t_{int} (pc)	17	16	14	15
c) RADII OF ONLY SNRS WHICH INITIATED SHOCK SYSTEMS, AT FIRST t_{cav}				
17.6 (%)	10	11	12	12
22.2 (%)	11	7	8	7
27.7 (%)	6	11	20	14
30 – 35 (%)	6	6	4	6
35 – 40 (%)	12	12	16	13
40 – 45 (%)	40	40	27	38
45 – 50 (%)	15	11	12	10
Average R_i at first t_{cav} (pc)	36	36	35	10

*This percentage of SNe occurred within preexisting cavities.

Table 6

Distributions of Effective Volumes of SNRs

V_{eff} Bin (10^5 pc^3)		Model* A	Model* B	Model* D
< 5	(%)	44	32	29
5 – 10	(%)	25	31	31
10 – 15	(%)	12	13	16
15 – 20	(%)	7	6	10
20 – 25	(%)	4	8	7
25 – 30	(%)	3	4	3
30 – 40	(%)	2	2	2
40 – 50	(%)	$\ll$1	0	0
> 50	(%)	2	3	3
Average V_{eff} (10^5 pc^3)		18	31	35

*Data for V_{eff} are not available for Model C.

FIGURE CAPTIONS

FIG. 1. — An idealized shock system consisting of a long cylindrical tunnel and a new SN inside. The inset shows an enlarged view of the wall. Gas parameters (see Table 2) are labeled for tunnels, walls, and ambient ISM. For a He abundance of 10%, $\rho_o \simeq 1.5 \times 10^{-24}$ g cm^{-3} and $\rho_w \simeq 2\,\rho_o$.

FIG. 2. — The evolution of (a) pressures P_i and (b) radii R_i for a pair of interacting SNRs, as it would be calculated within the numerical simulation. One SNR appears at time zero, represented by the lower solid curve in (a) and the upper curve in (b). The second SNR appears after 4×10^5 yrs at a distance of 60 pc from the first explosion, intersects at t_{int}, and completes a connection at t_{con}. The cavity shock pressure drop P_{cav} in the newer cavity, which occurs at t_{cav}, is calculated as explained in the text and is equal to the vertical distance between the end points of the dashed line. At t_{cav} the older cavity receives its pressure impulse, defined by the requirement that thereafter the two cavities are in pressure equilibrium with each other. After $t_{con} + \Delta t_{prop}$ the joint cavity expands uniformly to equilibrium with P_{ISM}.

FIG. 3. — The volume fraction in tunnels, averaged over Z, as a function of time for four simulated models with average porosities q as shown. Each point represents the fraction after ten time steps, and the number of SNe in the test space during that period is shown in the lower histograms. A burst of SNe is directly related to a surge in fraction, and the

isolated SNR lifetime and effective lifetime (from Table 3) are shown as an aid in interpreting the duration of the surges. The lower histograms appear different in all runs except C and D, although the input functions were the same, because ten time steps is a different fraction of the total time in each run.

FIG. 4. — The quasi-equilibrium tunnel fraction averaged over Z and time, as a function of Z-averaged porosity for several runs. The dashed line shows the relation expected without SNR interaction.

FIG. 5. — The tunnel fraction f(Z) and porosity q(Z) as functions of height above the plane, at the time a typical run (Model B) ended. q(Z) is an exponential with scale height 90 pc.

FIG. 6. — The number of SNRs with diameter less than D as a function of D. The line labeled $D^{2.5}$ corresponds to adiabatic blast waves and is the same as that drawn by Clark and Caswell (1976) to fit their sample of young "radio" SNRs. The points on the right are (unscaled) results for "X-ray" SNRs from the four simulation runs, not from observations. The dashed line (broken at the middle) is an extrapolation from the "X-ray" points down to the "radio" points; the former must be scaled by a factor of 10^3, roughly the volume ratio of galactic spiral arms to test space, in order to join the two halves of the line, showing that there is no basic inconsistency between radio observations and the simulation results. The line labeled D^4 illustrates the steepness of the

intermediate-diameter "X-ray" curves compared to the slope expected for SNR shells expanding according to momentum conservation.

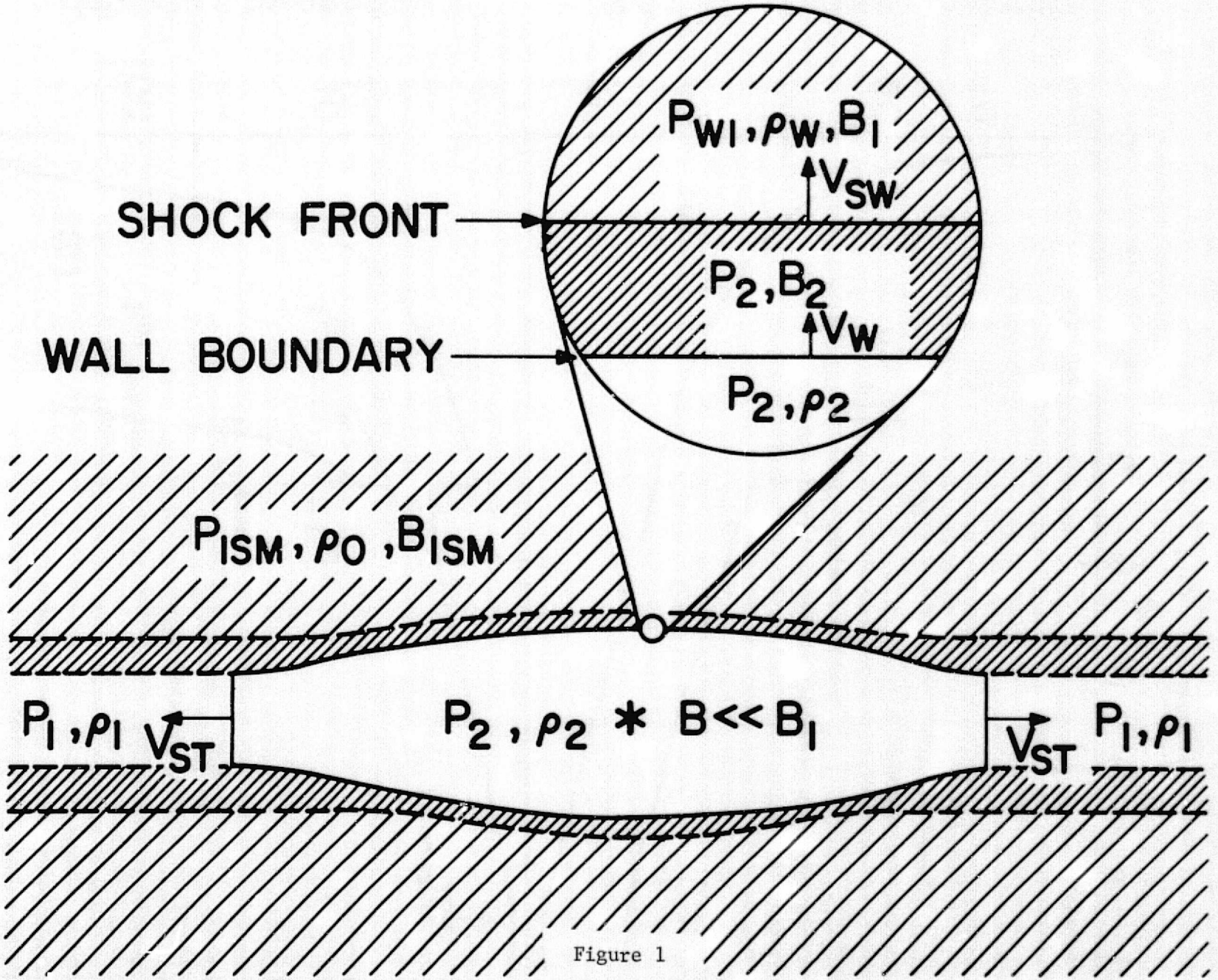

Figure 1

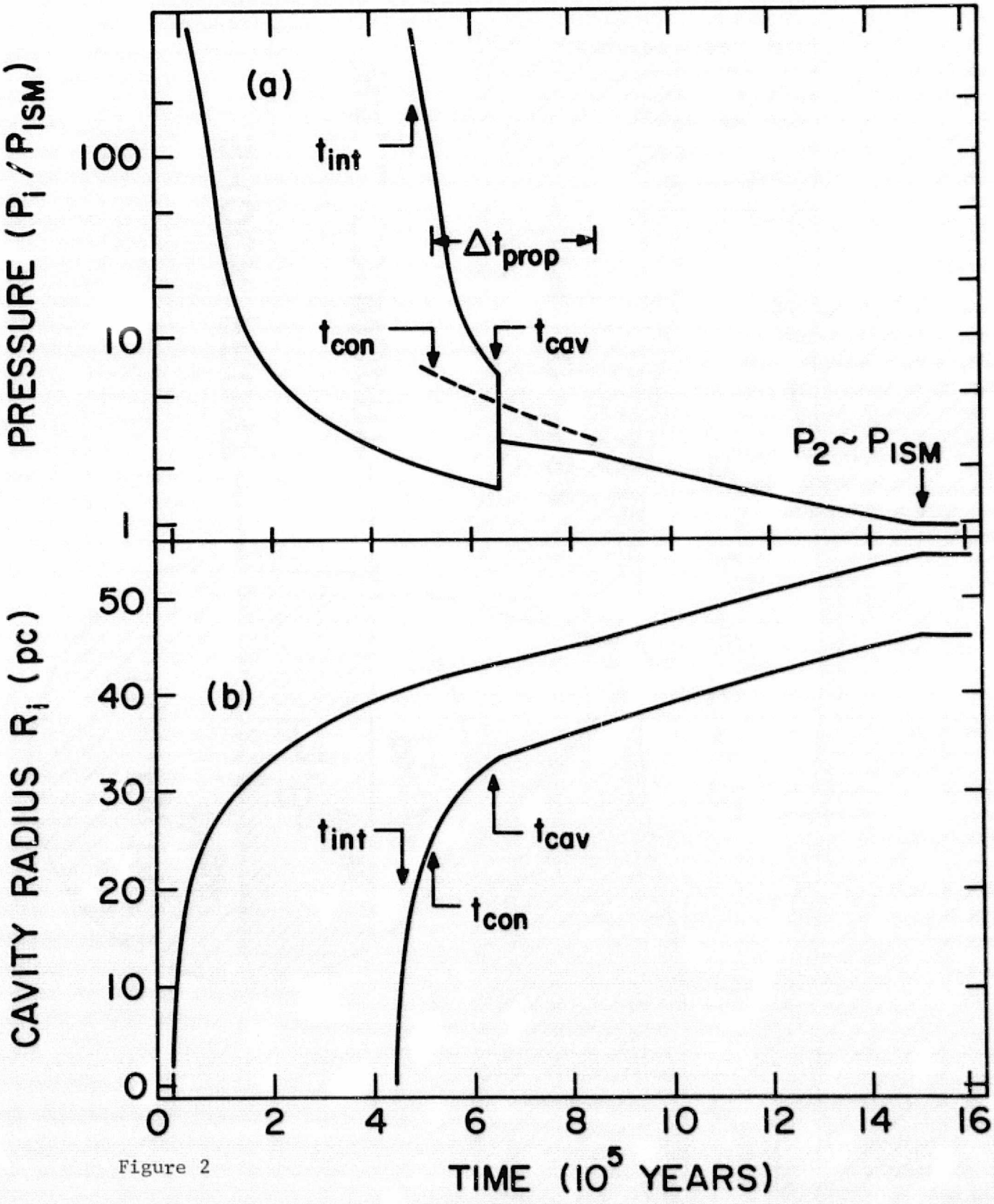
(a)
PRESSURE (P_i / P_{ISM})
100
10
1
t_{int}
Δt_{prop}
t_{con}
t_{cav}
$P_2 \sim P_{ISM}$
(b)
CAVITY RADIUS R_i (pc)
50
40
30
20
10
0
t_{int}
t_{cav}
t_{con}
0
2
4
6
8
10
12
14
16
TIME (10^5 YEARS)

Figure 2

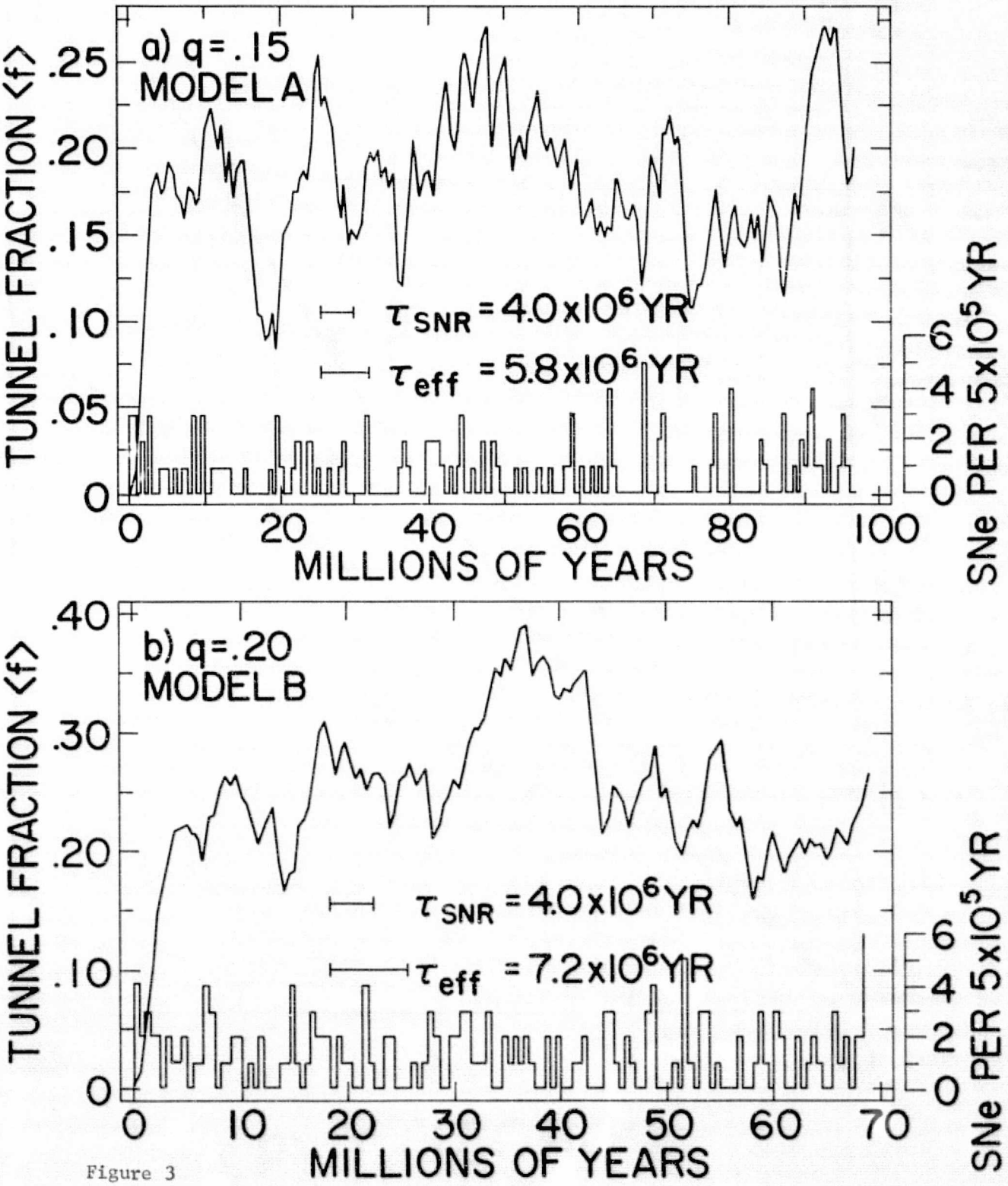
a) q=.15
MODEL A
TUNNEL FRACTION <f>
.25
.20
.15
.10
.05
0
τ_{SNR} = 4.0x10^{6}YR
τ_{eff} = 5.8x10^{6}YR
0
20
40
60
80
100
MILLIONS OF YEARS
SNe PER 5x10^{5}YR
6
4
2
0
b) q=.20
MODEL B
TUNNEL FRACTION <f>
.40
.30
.20
.10
0
τ_{SNR} = 4.0x10^{6}YR
τ_{eff} = 7.2x10^{6}YR
0
10
20
30
40
50
60
70
MILLIONS OF YEARS
SNe PER 5x10^{5}YR
6
4
2
0

Figure 3

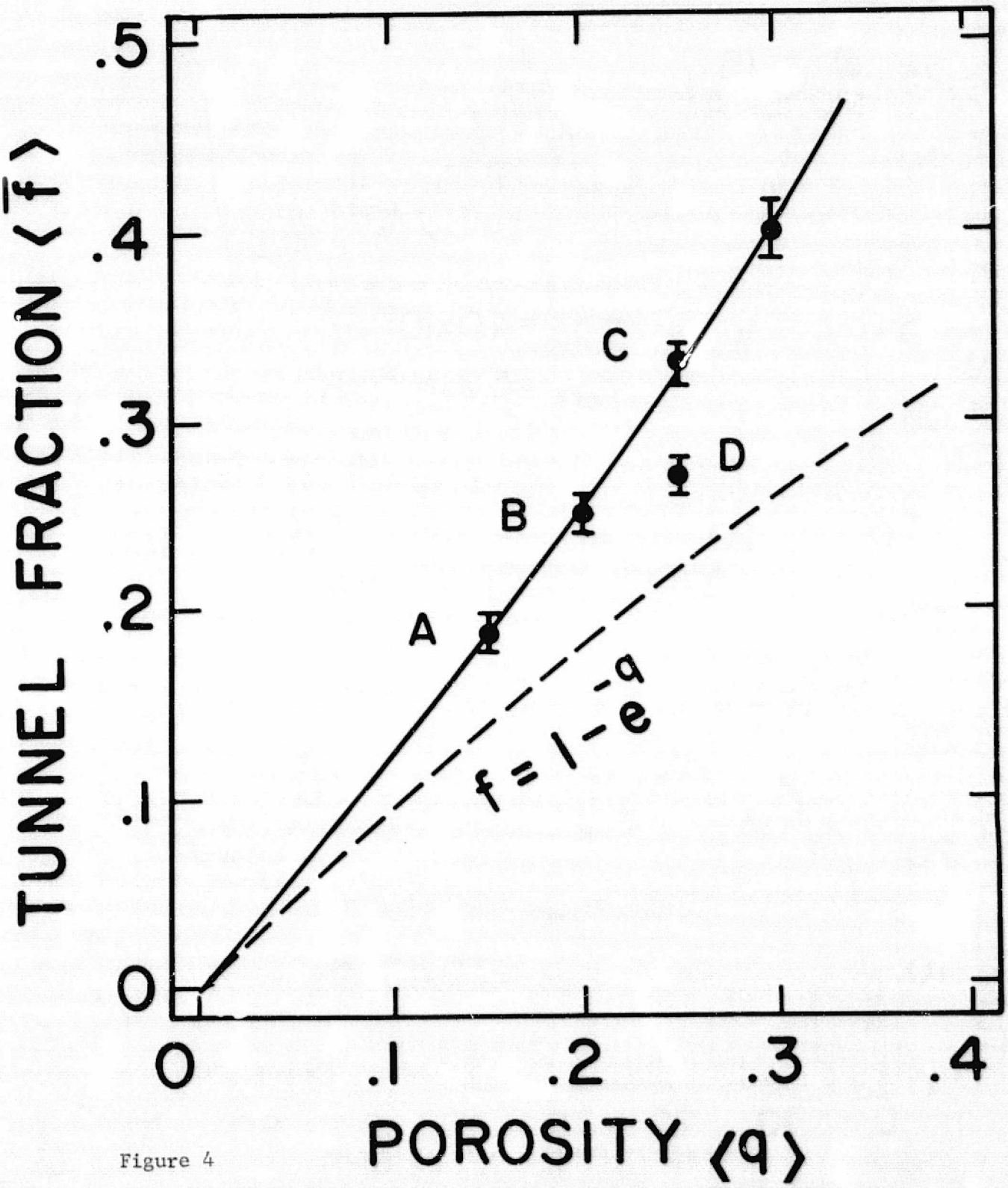

Figure 4

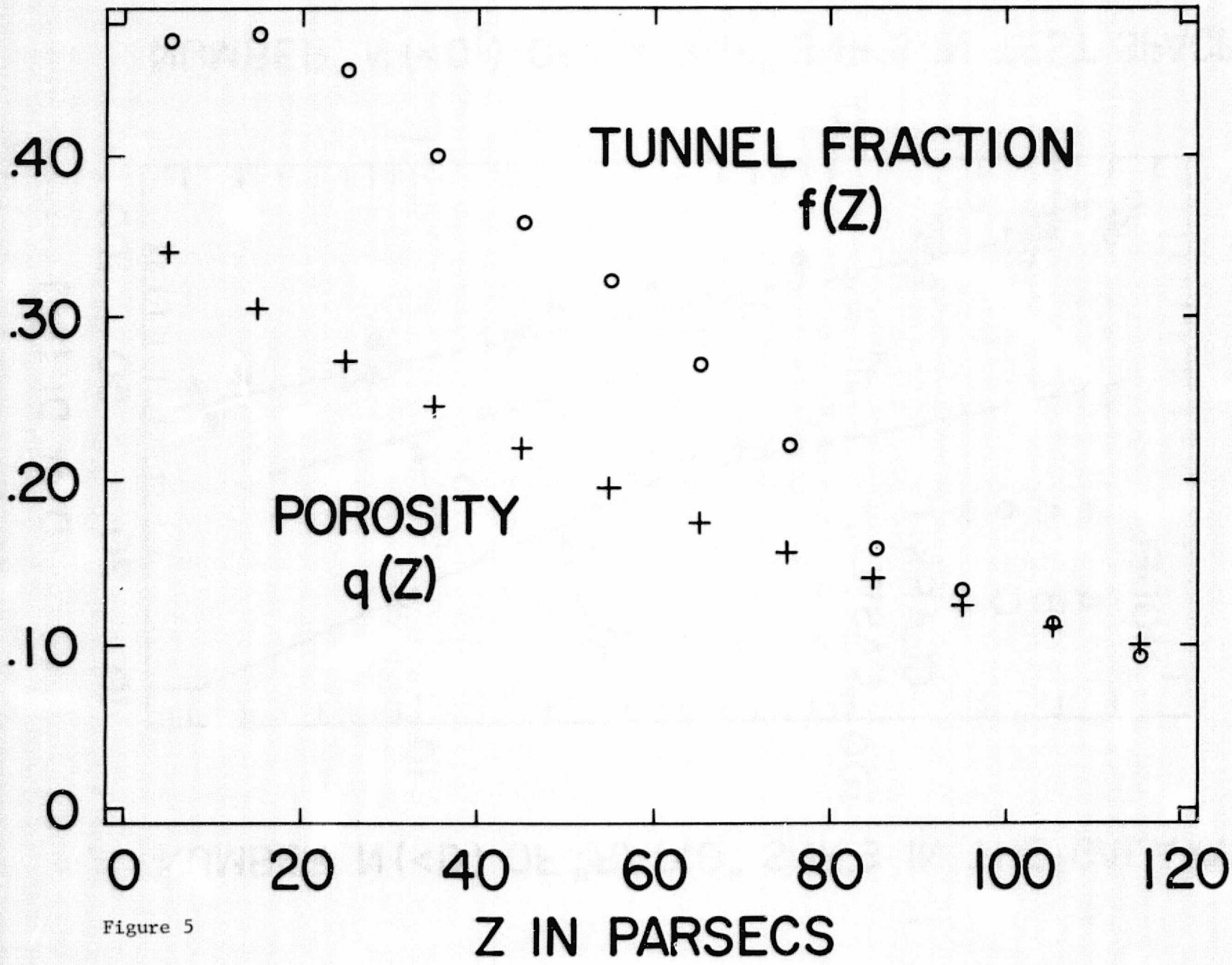
TUNNEL FRACTION
f(Z)
POROSITY
q(Z)
.40
.30
.20
.10
0
0
20
40
60
80
100
120
Z IN PARSECS

Figure 5

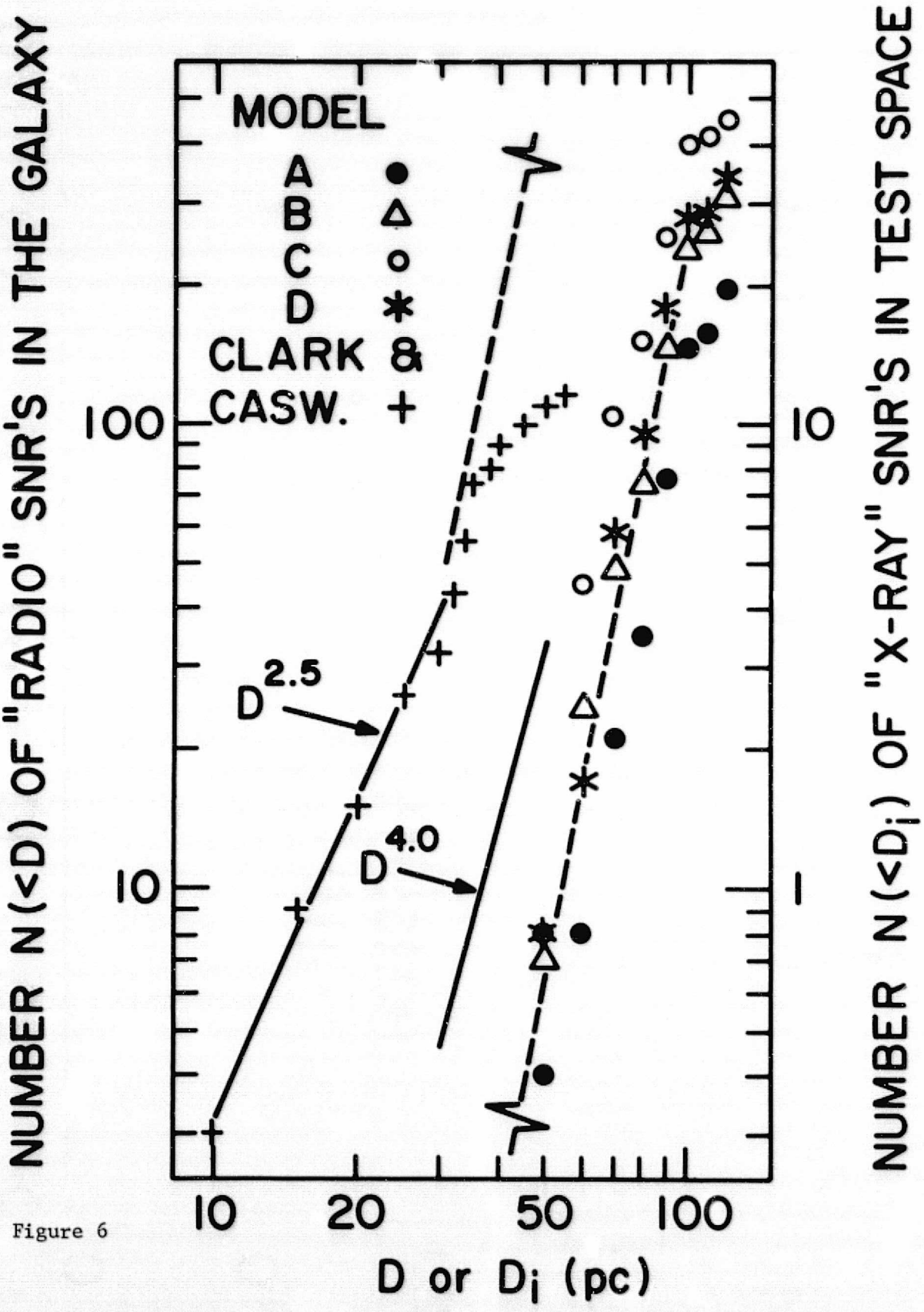
NUMBER N(<D) OF "RADIO" SNR'S IN THE GALAXY
NUMBER N(<Dᵢ) OF "X-RAY" SNR'S IN TEST SPACE
MODEL
A ●
B △
C ○
D ✱
CLARK & CASW. +
D^2.5
D^4.0
100
10
10
1
10
20
50
100
D or Dᵢ (pc)

Figure 6